Macromolecules

pubs.acs.org/Macromolecules Article

Local Water Transport in Rubbery versus Glassy Separation Membranes and Analogous Solutions

Andrew G. Korovich, Kevin Chang, Geoffrey M. Geise, and Louis A. Madsen*

Cite This: *Macromolecules* 2021, 54, 11187–11197 Read Online

ACCESS | Metrics & More | Article Recommendations | Supporting Information

ABSTRACT: To probe local molecular-scale effects of polymer backbone dynamics on the transport of water and salt in desalination membranes, we have studied water diffusion behavior in two chemically similar copolymers using NMR diffusometry. We observe a greater activation energy for water diffusion in a glassy hydroxylated methacrylate membrane as compared to its chemically similar rubbery acrylate counterpart. We also investigate water diffusion in aqueous solutions of both precursor monomers, which serve as close mimics of each membrane's local environment. Comparison between membranes and solution mimics can further inform on the effects of purely geometric (physical) nanoconfinement versus those effects from water–chain intermolecular interactions. We find that diffusive activation energy differences between the rubbery and glassy membranes originate mainly from differences in the intermolecular interactions of water with the different local polymer structures. We further propose that the more rigid glassy methacrylate backbone introduces configurational restrictions to transport, leading to greater water–salt permeability selectivity compared to the rubbery polymer.

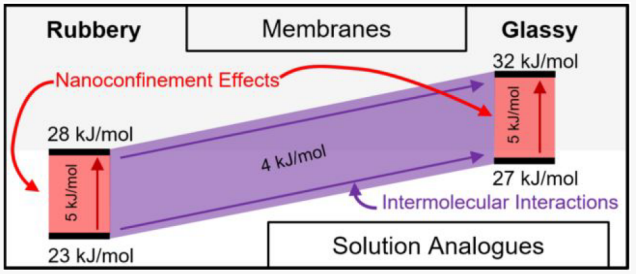

INTRODUCTION

To address current and future global water shortages, polyamide-based membranes are the current "gold standard" in reverse osmosis water purification technology because of their simultaneously high water flux (20–40 L m^{-2} h^{-1}) and salt rejection (>99%).[1−6] However, these materials face shortcomings in the form of fouling and oxidative degradation due to the chlorine use necessary for pretreatment of feedwater.[2−7] While many different avenues are being explored to produce efficient chlorine-resistant materials, largely through synthesis of polysulfone- and poly(phenylene oxide)-based membranes,[8−10] these materials presently are unable to match the performance of polyamide membranes. Further advances in membrane design require studies into structure–dynamics–property relationships to achieve the combination of desirable properties needed to meet water purification goals of the future.[11,12]

To delve deeper into structure–dynamics–property relationships, we have investigated two chemically similar materials: a methacrylate-based hydroxymethyl methacrylate-*co*-methyl methacrylate (HEMA-*co*-MMA) with a *glassy* backbone and an acrylate-based hydroxyethyl acrylate-*co*-ethyl acrylate (HEA-*co*-EA) with a *rubbery* backbone (Figure 1). Similar to commercial polyamide reverse-osmosis membranes, these materials absorb roughly 10 % water by mass. This low water content and its similarity to that of commercial materials are important because water content strongly influences water and salt transport in hydrated polymers.[7,13] The dynamics of the polymer backbone play a more significant role in low-water-content materials due to an increased degree of interaction between water, salt ions, and the polymer in the small (~1 nm) hydrophilic pathways that facilitate transport through the membrane. This situation contrasts materials like Nafion, which at higher hydration levels shows the presence of "bulk-like" water or regions where water–water interactions dominate the transport behavior.[14,15]

Our previous studies of HEMA-*co*-MMA and HEA-*co*-EA have provided insight into the effects of polymer backbone dynamics on water and salt transport through these membranes over a range of length scales by NMR diffusometry.[7] We have seen greater water–salt selectivity in HEMA-*co*-MMA membranes compared to that in HEA-*co*-EA as well as increasing water–salt selectivity in the HEMA-*co*-MMA materials with increasing size of the salt ions.[16] Measurements of water diffusivity on the micrometer length scale allowed us to separate the *tortuosity* of the membrane hydrophilic network into two regimes. One tortuosity corresponds to an average over larger scale heterogeneities (~0.5 μm and larger), and one tortuosity includes the local structure and morphology responsible for the selective

Received: August 19, 2021
Revised: November 3, 2021
Published: November 17, 2021

https://doi.org/10.1021/acs.macromol.1c01746
Macromolecules 2021, 54, 11187–11197

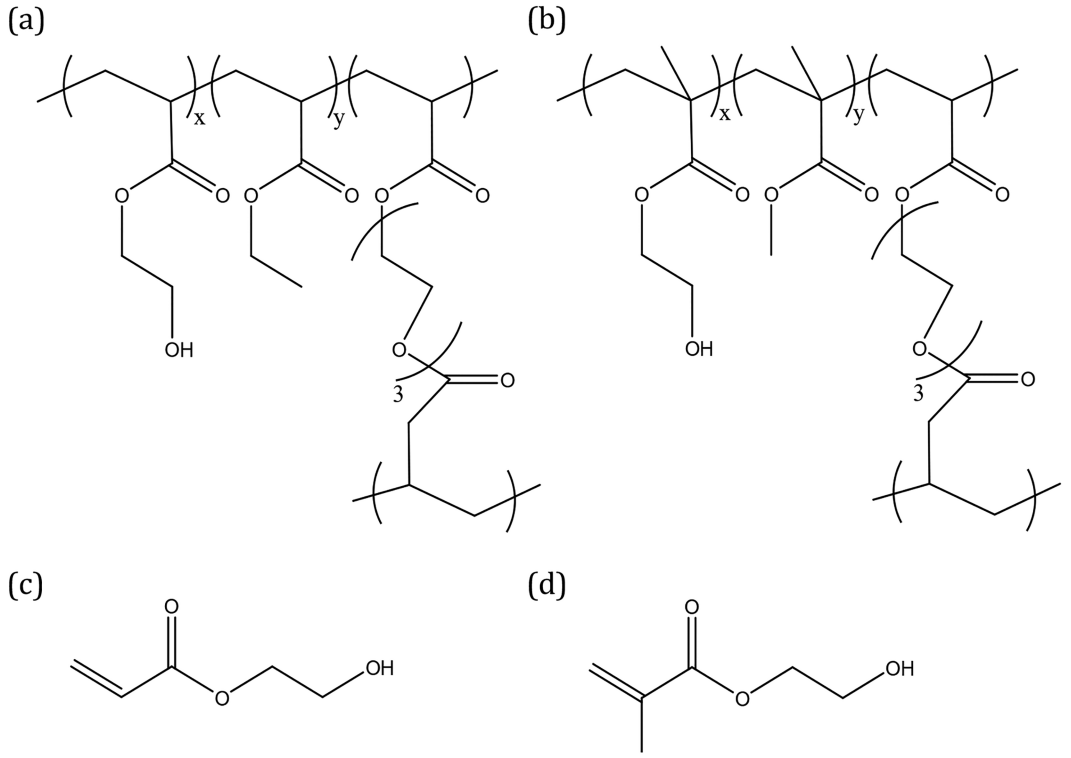

Figure 1. Chemical structures of the (a) HEA-*co*-EA and (b) HEMA-*co*-MMA materials, both created through a photoinitiated polymerization process with 3 mass % poly(ethylene glycol) diacrylate (PEGDA) included for cross-linking. The ratio of hydrophilic to hydrophobic comonomers of these materials is represented on the structures as *X* and *Y* (i.e., HEA-*co*-EA contains an *X*:*Y* ratio by mass of HEA:EA), where 35:65 is typical for both materials. These chemically similar membranes differ predominantly in that (a) is rubbery and (b) is glassy in the hydrated state. Aqueous solutions of the (c) HEA and (d) HEMA monomers provide models for the local intermolecular environment of the internal hydrophilic transport pathways present in the two copolymers.

transport of salt on the molecular level.[7,17] Because of practical limitations of NMR diffusometry (pulsed-field-gradient switching times), we cannot directly probe the contribution to diffusion on shorter length scales (<100 nm). Therefore, we need another approach to better understand the local interactions and structure that differentiate the selectivity of these two materials.

The activation energy (E_a) of diffusion is affected by molecular scale (~1 nm in length, ~1 ps in time) interactions that influence diffusion.[14,18−22] These interactions include not only those that are *chemical* in nature (e.g., hydrogen bonding and dipole−dipole interactions) but also those that are *physical* restrictions to diffusion (also termed geometric nanoconfinement).[18] In separations (e.g., desalination) membranes, the boundaries or restrictions to molecular motion between hydrophilic and hydrophobic regions of the polymer can give rise to geometric nanoconfinement. We use the Arrhenius equation (eq 1) to extract the E_a of diffusion

$$D = D_0 e^{-(E_a/RT)} \quad (1)$$

where D is the diffusion coefficient, D_0 is the pre-exponential factor, T is the absolute temperature, and R is the gas constant.

As the HEMA-*co*-MMA and HEA-*co*-EA membranes studied here sorb only a small amount of water at saturation (~10 wt %), the hydrophilic medium through which water diffuses will be strongly influenced by intermolecular interactions due to the hydrophilic moieties present at high density. Previously, Lingwood et al.[14] and Zhang et. al[18] have studied trifluoromethanesulfonic acid and lithium trifluoromethanesulfonate, respectively, as local molecular mimics for the ion-dense environment of perfluorosulfonic acid membranes such as Nafion. These studies were therefore able to separately address the effects of confinement on water transport. In the present work, we use a similar strategy to quantify the effects on water diffusion originating from the intermolecular interactions of water and the effects from geometric confinement. In our previous paper on these materials,[7] we made the experimentally convenient approximation that at the limit of very short diffusion length scales water molecules do not experience any restricted diffusion effects as a result of the polymer membrane. Pure water was therefore used as a model for the local diffusion behavior to determine our reported membrane tortuosity values.

The use of pure water as a model for local diffusion, however, neglects the significant impact that intermolecular interactions between water and the hydrophilic moieties can impart to the diffusion behavior, even in the absence of any nanoconfinement (membrane physical matrix) effects. To probe a more appropriate analogue to the chemical environment within the polymer membranes, we perform diffusion measurements on mixtures of water and each hydrophilic monomer (HEMA and HEA) at water:monomer mole ratios equivalent to what exists inside the hydrated membranes (2.8 water molecules per HEA monomer and 3.6 water molecules per HEMA monomer). These analogues allow us to observe the impact, on water diffusion, of intermolecular interactions between water and the hydrophilic moieties, and without the geometric confinement effects present in the membranes. These solutions also allow for a second point of comparison

https://doi.org/10.1021/acs.macromol.1c01746
Macromolecules 2021, 54, 11187−11197

regarding the assumed similarity in chemical interactions between HEMA and water versus HEA and water. From this information, we can better define the structural features that control the differences in transport selectivity between the glassy HEMA-*co*-MMA and the rubbery HEA-*co*-EA membranes. We propose that this methodology can be applied to understand chemical and physical contributions across multiple length scales that affect bulk transport in a range of polymeric materials.

In addition to measuring diffusion and its associated activation energy, NMR can be used to elucidate information about the dynamics of chemical exchange.[23−32] In these systems, interactions between water protons and the hydroxyl groups of the hydrophilic moieties can enable exchange of labile protons between the two species.[25,28,30] This exchange results in temperature-dependent broadening and coalescence of the NMR signals arising from the exchanging sites as well as changes in the chemical shift, a property that can be used as an "NMR thermometer".[33] While the polymer and water NMR signals inside the *membranes* are broad and thus obscure such dynamics, the *monomer solution* signals reveal clear chemical exchange. From these observations, we present additional insight into how molecular structural differences between HEMA and HEA affect how these two chemical species interact with water.

EXPERIMENTAL SECTION

Polymer Sample Preparation. The two copolymer membranes investigated (Figure 1) were prepared according to the procedures discussed in Chang et al.[7] The 35:65 HEA-*co*-EA membrane was cut into 3 mm diameter discs, stacked in groups of 16 disks, and wrapped with thin strips of PTFE tape to hold them together, before being equilibrated in 0.5 M NaCl solution until saturated. The 35:65 HEMA-*co*-MMA material was too brittle to be neatly cut by using the circular punch used for the HEA-*co*-EA material and instead was cut with a blade into rectangular sections approximately 3 mm × 4 mm. The slices were stacked and wrapped in a similar manner to the HEA-*co*-EA discs, before being similarly equilibrated in 0.5 M NaCl solution until saturated. The membranes were 200 μm thick. The equilibrium water content in each material was as previously reported,[7] with HEA-*co*-EA absorbing 8.2 ± 0.4 mass % and HEMA-*co*-MMA absorbing 9.1 ± 0.5 mass %. For the NMR experiments, the stacks were removed from the equilibration solution, blotted to remove any surface water, and wrapped completely with additional PTFE tape to minimize water loss to evaporation. The wrapped stacks were sealed inside a polyoxymethylene (POM) sample cell designed to minimize excess volume to prevent water loss from the sample through evaporation.[19,34,35]

Solution Sample Preparation. The polymer-analogous solution samples were prepared by mixing the same monomer reagents used in the polymerization process, with HPLC grade water (Fisher Chemical). Approximately 1 mL aliquots of the solutions were added to 5 mm NMR tubes, along with four 0.8 × 1 × 10 mm^3 (inner diameter, outer diameter, and length, respectively) glass capillary tubes to mitigate the effects of convection on the diffusion experiments at elevated temperatures. The NMR tubes were additionally flame-sealed to prevent evaporative loss of the solution and stored in an opaque container to prevent photopolymerization of the acrylate monomers over time. Solution concentrations were confirmed by NMR integrations.

NMR Diffusometry. Water diffusion measurements were performed, for both the copolymer samples and the monomer−water solutions, on a 9.4 T Bruker Avance III wide-bore spectrometer, by using the monopolar pulsed-gradient stimulated echo (PGSTE) pulse sequence. A Bruker Diff60 diffusion probe was used with a 5 mm radio-frequency (RF) coil for all NMR diffusion measurements of the membrane materials. A Diff50 gradient coil was used for diffusion measurements of the solutions; good agreement was found with identical experiments run on the Diff60 coil. Equation 2 shows the relation between the normalized signal intensity data (I/I_0) obtained from a PGSTE experiment and the Stejskal−Tanner parameter, b, which is used to extract the measured diffusion coefficient, D, from a plot of I/I_0 versus b:

$$\frac{I}{I_0} = e^{-bD} = e^{-D\gamma^2\delta^2 g^2(\Delta-\delta/3)} \tag{2}$$

The Stejskal−Tanner parameter, b, is composed of the following experimental parameters and constants: the effective gradient pulse length, δ, the gradient strength, g, the gyromagnetic ratio of the nucleus being observed, γ, and the experimental diffusion time, Δ. The strength of the magnetic field gradients was calibrated by using a sample of 1 wt % H_2O in D_2O, which has a known diffusion coefficient of 1.91 × 10^{-9} m^2 s^{-1} at 25 °C. Measurements performed on membrane samples used a 90° pulse time of 5 μs, and a linear gradient list with gradient strengths from 20 to 350 G/cm and 40 to 800 G/cm for water in the HEA-*co*-EA and HEMA-*co*-MMA samples, respectively. An effective gradient pulse duration of 1−2 ms (actual pulse duration is 1.57 times the effective duration for the sinusoidal pulse shape used) and a diffusion time of 20 ms were used for all diffusion measurements, with repetition times of 3−5 s. For all diffusion experiments, four dummy gradient pulses and four dummy scans were utilized to minimize signal weighting artifacts.

Diffusive Activation Energy. Water diffusion measurements were performed at varied temperatures, ranging from 15 to 55 °C for the copolymer samples and −10 to 65 °C for the solution samples. Note that as evaporation and sample freezing are more easily observed in a solution sample, a wider window could be used, assuming transverse relaxation time (T_2) values are long enough at lower temperature. Activation energies are found from the slope of the linearized Arrhenius plot of the diffusion coefficient versus inverse temperature. As a verification that no measurable convection was occurring in the solution samples measured at elevated temperatures, a convection-compensated double stimulated echo experiment[36] was run at the highest temperature, and good agreement was found with the single stimulated echo results. Note that because of the short T_2 of the exchange-broadened OH−water signal, this experiment could not be run at all temperatures. For most polymeric systems, the conventional PGSTE is suitable for measurement of the widest range of samples (with short T_2) and with negligible phase artifacts (from convective flow), since polymer matrices will effectively block any substantial convection pathways.

NMR Sample Temperature Calibration. Temperature calibration was performed by using glass-sealed samples of neat ethylene glycol (anhydrous, 99.8%, Sigma-Aldrich) at temperatures above 30 °C and methanol (anhydrous, 99.8%, Acros Acroseal) containing 0.03 vol % HCl (37%, Sigma-Aldrich) for temperatures below 30 °C. Both calibration standards were filled to a similar height as the solution samples to ensure that the observed temperature of the standard was identical (±1 °C) to the diffusion samples. For temperatures between 30 and 110 °C, the chemical shift difference, $\Delta\delta$, between the two peaks exhibited by pure ethylene glycol in ^{1}H NMR can be related to the temperature, T, of the sample by eq 3:[33,37]

$$T\ (\mathrm{K}) = \frac{4.637 - \Delta\delta}{0.009967} \tag{3}$$

Between −70 and 30 °C, eq 4 describes the relationship between the chemical shift difference and temperature for methanol.[38]

$$T\ (\mathrm{K}) = -23.832\Delta\delta^2 + 29.46\Delta\delta + 403 \tag{4}$$

Chemical Exchange Measurements. The 1D NMR spectra of the monomer solutions were obtained over a temperature range of −50 to 70 °C on a 600 MHz Bruker Avance III spectrometer equipped with a 5 mm triple resonance TBI probe. The samples were allowed to equilibrate at each temperature for a minimum of 15 min before acquisition of the final spectrum to ensure an accurate representation of the exchange behavior at that temperature.

https://doi.org/10.1021/acs.macromol.1c01746
Macromolecules 2021, 54, 11187−11197

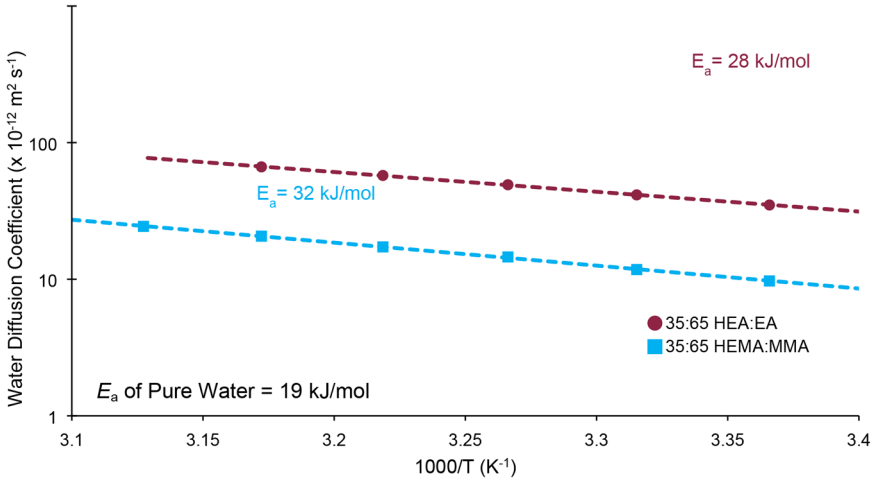

Figure 2. Linearized Arrhenius plot of water diffusion in saturated HEMA-*co*-MMA (blue, square) and HEA-*co*-EA (maroon, round) membrane materials. Water in the HEA-*co*-EA material shows both faster overall transport (3.5×10^{-11} m^2/s at 25 °C) and a lower activation energy for diffusion (E_a = 28 ± 1 kJ/mol) than the HEMA-*co*-MMA material (1×10^{-11} m^2/s at 25 °C and E_a = 32 ± 1 kJ/mol). Thus, the local (∼1 nm) barriers to diffusion are higher in the HEMA material. The uncertainty in the diffusion coefficients measured is ca. ±3%.

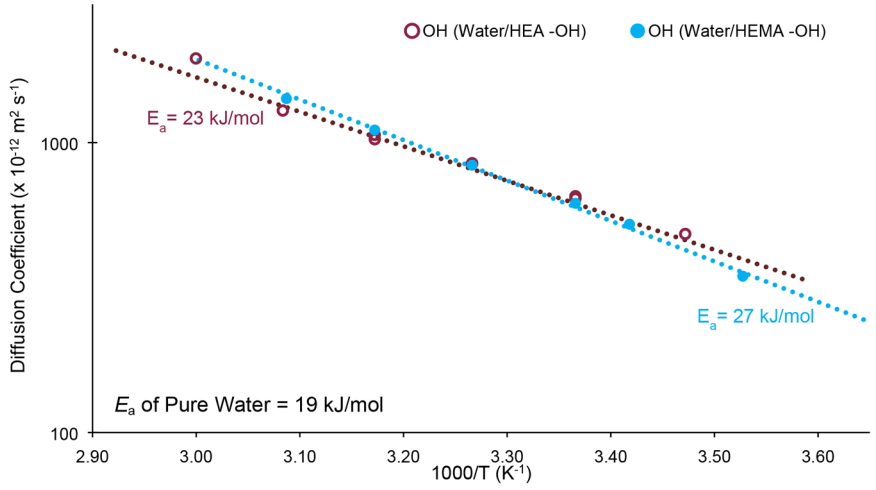

Figure 3. Linearized Arrhenius plot of water and monomer diffusion in the 2.8:1 H_2O:HEA (blue, solid symbols) and 3.6:1 H_2O:HEMA (maroon, hollow symbols) solutions, which represent analogues to the environments of their respective membranes. We find the E_a for water to be 23 ± 2 kJ/mol (HEA−water solution) and 27 ± 1 kJ/mol (HEMA−water solution). The uncertainty in the measured diffusion coefficients is ca. ±5%.

Experiments utilized a relaxation delay of 10 s, four dummy scans, eight acquisition scans, a 90° pulse time of 10 μs, and acquisition times from 0.2 to 3 s, adjusted for the length of the free induction decay at a given measurement temperature.

RESULTS AND DISCUSSION

Activation Energy of Diffusion Studies. To advance our understanding of how local intermolecular interactions and geometric nanoconfinement separately contribute to bulk diffusion in these materials, we use variable temperature NMR diffusometry to probe activation energy (E_a) in the two membranes. Using the Arrhenius plot of Figure 2, we find the E_a of water diffusion in the HEA-*co*-EA membrane to be 28 ± 1 kJ/mol, while in the HEMA-*co*-MMA membrane E_a = 32 ± 1 kJ/mol.

The greater E_a observed for water in the HEMA-*co*-MMA material suggests that interactions between water molecules and the surrounding polymer are stronger than in the HEA-*co*-EA material. E_a reflects the average energy landscape given by the local (∼1 nm) physical and chemical interactions that average over the prediffusive (inertial) motion regime.[14,18] Thus, confinement by the hydrophobic regions of the polymer, combined with barriers or obstacles (e.g., physical restrictions by polymer chains) and with intermolecular effects (e.g., hydrogen bonding and dipole−dipole interactions), provide the major contributions to E_a values. The observed E_a values are comparable to those measured for water diffusion in acid form[14,22] and lithium form[18] Nafion at similar levels of hydration.

In addition to the E_a of diffusion, the pre-exponential factor, D_0, provides information related to the configurational degrees of freedom available for diffusive motion.[18] We find that while water diffusion in the HEMA-*co*-MMA material is more energetically hindered (high E_a), the configurational environment available for transport[14,19] is slightly less constrained than that of the HEA-*co*-EA material, with D_0 values of 4.4×10^{-6} and 2.6×10^{-6} m^2 s^{-1}, respectively. Based on the overall D values and the diffusion time (Δ) of the NMR diffusometry experiments, the diffusion length (root-mean-squared displacement) of water molecules in these measurements is 0.5−3 μm.

https://doi.org/10.1021/acs.macromol.1c01746
Macromolecules 2021, 54, 11187−11197

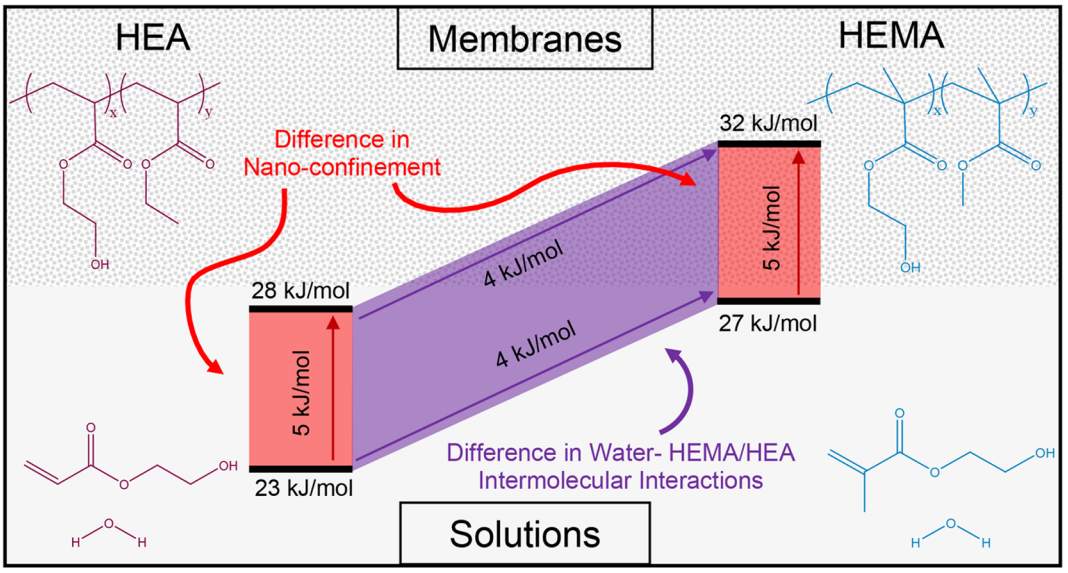

Figure 4. Comparison of the diffusive E_a of water in both membranes (top left, HEA-*co*-EA; top right, HEMA-*co*-MMA) and the membrane analogue solutions (bottom left, HEA−water solution; bottom right, HEMA−water solution). As the two membrane analogue solutions mimic the local molecular environment of their respective membranes (absent any physical confinement), the difference in E_a seen between these pairs (HEA-*co*-EA + HEMA-*co*-MMA and HEA−water + HEMA−water) should reflect the contribution to E_a resulting only due to geometric nanoconfinement. Similarly, as the only differences between the two analogue solutions is the result of chemical intermolecular interactions and concentration, the difference in E_a between these solutions reflects this. Interestingly, the difference in water E_a observed between the two membranes matches that between the two solutions, and the differences from each solution to their respective membranes match as well. This suggests that the hydrophilic network of the membranes exhibits a very similar degree of confinement on water diffusion and at the ∼1 nm scale differs only due to intermolecular interactions between water and the hydrophilic monomer moieties.

The diffusion coefficients D, along with D_0 measured here, are additionally sensitive to the micrometer-scale membrane morphology we have previously reported, complicating interpretation of the differences in D_0 that arise solely from local contributions. Additionally, because of the large uncertainty in the extrapolation of D_0 values, we compare only the relative differences between D_0 values and not the absolute values. Comparison with the D_0 values measured for the analogous solutions provides additional clarity and will be discussed below.

The observed differences in the E_a of water agree with our previous work,[7] in which we found that the degree to which structural heterogeneities and restrictions affect the bulk diffusion through the membrane was similar between the HEMA-*co*-MMA and HEA-*co*-EA materials. Water diffusion in the HEMA-*co*-MMA membrane was slower (1×10^{-11} m^2/s at 25 °C) on the micrometer length scale than in the HEA-*co*-EA membranes (3.5×10^{-11} m^2/s at 25 °C). From the measurements of the water E_a in the membranes, we cannot separate the effects on transport due to differences in intermolecular interactions between water and HEMA or HEA units from the effects of nanoconfinement and polymer morphology. Thus, another point of comparison is needed.

To observe the effects on water transport due to differences in chemical interactions between water and the respective hydrophilic monomers, we measured the E_a of diffusion in two membrane analogue solutions. We prepared these solutions at water:monomer concentrations that match the internal environment of the membranes reported in our previous work (2.8 water molecules per HEA unit and 3.6 water molecules per HEMA unit). These solutions thus mimic the local intermolecular environment of the membrane hydrophilic networks, and in the absence of any geometric confinement or membrane tortuosity effects.[7]

From these diffusion studies (Figure 3), we find that water in the HEA analogue solution has $E_a = 23 \pm 1$ kJ/mol, whereas the HEMA analogue solution has $E_a = 27 \pm 1$ kJ/mol. Additional diffusion measurements, including D values for the monomer species, are shown in Figure S1. The activation energies measured for these solutions follow the trend seen for the membrane materials: water diffusion experiences a lower energetic barrier to diffusion in the HEA−water solution, while the HEMA−water solution is more energetically hindered. Here, the D_0 values observed reflect the local configurations available to the diffusion process, and we see that water in the HEMA analogue solution has a higher D_0 (2.9×10^{-5} m^2 s^{-1}) as compared to the HEA solution (6.2×10^{-6} m^2 s^{-1}). As a result, the magnitude of the overall water D values for the two analogue solutions are similar (±10%) across the temperature range studied.

Interestingly, if we compare the difference in water E_a between the membrane analogue solutions and their respective membranes, we see that they are identical (Figure 4). Similarly, differences in water E_a from HEA to HEMA match for the same sample type (solution or membrane). From these similarities, we propose that the local scale (∼1 nm) diffusion of water in these two membrane materials is affected very similarly with regards to nanoconfinement effects and only differs because of the difference in intermolecular interactions (including dynamics) between water and the two hydrophilic monomers. Given that these two materials are made from similar comonomers and hydrophilic:hydrophobic monomer ratios, similar cross-linking densities, and polymerization methods, it appears that there are similar confinement effects due to the local polymer structure on water diffusion.

https://doi.org/10.1021/acs.macromol.1c01746
Macromolecules 2021, 54, 11187−11197

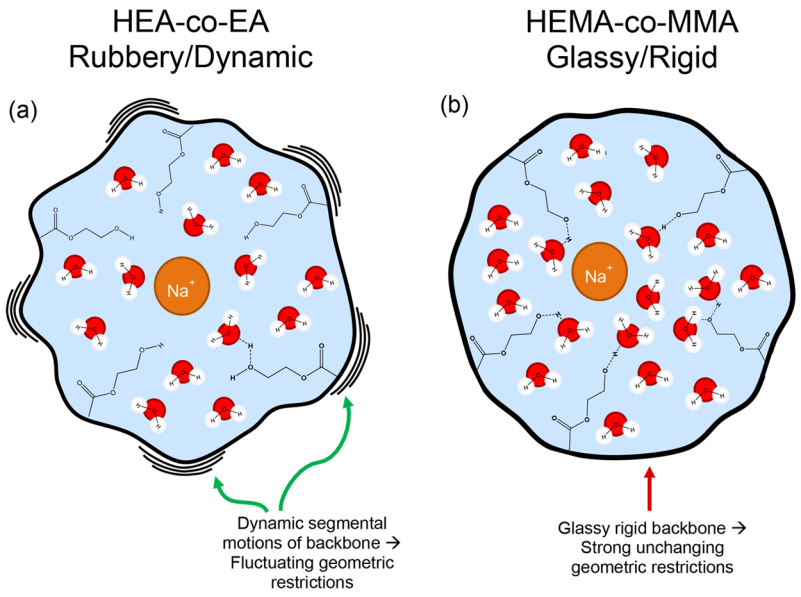

Figure 5. Illustration of the different local environments of the hydrophilic network in the rubbery HEA-*co*-EA (a) and glassy HEMA-*co*-MMA (b) membrane materials. We propose that the more dynamic chains of HEA-*co*-EA allow for greater configurational freedom in the diffusion of salt and water, which, in addition to the weaker intermolecular interactions, results in a system where both salt and water can diffuse more freely as compared to HEMA-*co*-MMA. The rigid methacrylate backbone of HEMA-*co*-MMA disrupts the cooperative motion of polymer chains with water and salt molecules, reducing the configurational degrees freedom of available, which in combination with the greater energetic hindrance results in greatly slowed transport of the relatively large, solvated ions and thus higher water−salt selectivity.

However, this is not something that could be immediately assumed due to the very different dynamics of the polymer backbones, as evidenced by their glass transition temperatures of −20 °C (HEA-*co*-EA) and 80 °C (HEMA-*co*-MMA).[7] Considering the similarity in energetic penalty of geometric confinement between the two materials, it appears that the *local transport behavior of the membranes* will match the similarity in the *overall water diffusivity* observed in the two *solutions*. The D_0 values measured for water in the membrane materials, though affected by micrometer-scale heterogeneities (morphology), show a slightly greater configurational freedom in HEMA-*co*-MMA, following the observations of the overall D of the analogous solution. If the local D_0 for water in the membranes (that is, the D_0 that would be measured if no micrometer-scale heterogeneities were present) is closer to the values seen in solution, then the magnitudes of water diffusion on the local molecular scale in the two materials should be similar, even though the energetics of the diffusion process are different.

HEMA versus HEA: Effects on Salt Selectivity. Previously, we have reported on the water and salt sorption, diffusivity, and permeability selectivity in these materials.[7,16] The glassy HEMA-*co*-MMA exhibits greater diffusivity, water E_a, and permeability selectivity (Figure S2) and shows increasing selectivity as the size of the salt species is increased. We attributed this to the rigid polymer backbone of the HEMA-*co*-MMA material forming a more tightly confined, hydrophilic (confinement) network, which presumably slows transport of salt ions to a greater degree than water molecules due to their (hydrated) size. However, the water E_a values presented here indicate a similar energetic penalty due to nanoconfinement in both HEMA and HEA materials. Furthermore, the pre-exponential factor D_0 determined for these solutions reflects greater configurational degrees of freedom in the diffusion process for the HEMA solution (vs HEA), as we also observe for water in the HEMA-*co*-MMA membrane (vs HEA-*co*-EA), leading to similar overall water diffusivity for both HEMA and HEA materials.

Figure 5 depicts a proposed model to resolve this apparent paradox. In the membrane environment, the HEMA monomers are more fixed in their arrangement and orientation due to the glassy polymer backbone anchoring them, which could disrupt the configurational freedom for hydrated salt ion motions and thus cause a lower D_0 for salt ions. In HEMA, decreased configurational freedom combined with the larger energetic penalty for diffusion should hinder the transport of water-solvated salt ions to a greater degree than in HEA-*co*-EA. In the HEA material, the more dynamic polymer backbone should allow for chain movement and reorientation such that more configurational freedom is available to water molecules and salt ions. Interestingly, these issues of diffusion energetics and configurational freedom may be sensitive to the specific chemistry of the polymer and the diffusing molecules. For example, local water diffusion coefficients studied by quasi-elastic neutron scattering were observed to be much faster and nearly bulk-like in a highly cross-linked and rigid polyamide, whereas water diffusion in a structurally more open anion exchange membrane was slower.[39] This study along with our results presented here highlights the need to consider both dynamics and molecular interactions when studying small molecule transport in polymers. Future studies will focus on unraveling these diffusion effects directly for dissolved salt ions with varying size.

Material Tortuosity on Local-Micrometer Length Scales. Previously we described two regimes of material tortuosity: one for local-to-bulk (>1 μm) length scales ($\mathcal{T}_{L-B}$) and one for micrometer-to-bulk length scales ($\mathcal{T}_{M-B}$).[7] The local diffusion coefficient, D_{loc}, in the local−bulk tortuosity was represented by that of pure water at 25 °C. This made the (admittedly simplified) assumption that as the average

https://doi.org/10.1021/acs.macromol.1c01746
Macromolecules 2021, 54, 11187−11197

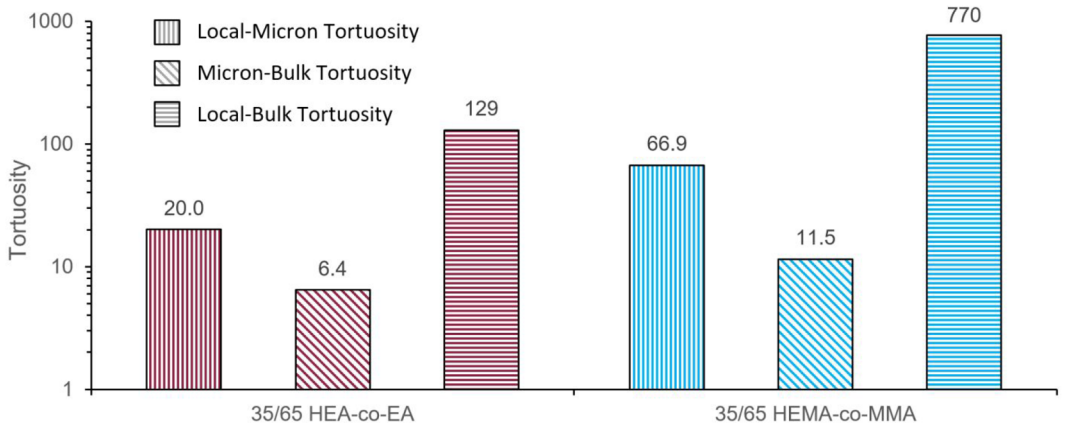

Figure 6. Material tortuosities for the HEA-*co*-EA and HEMA-*co*-MMA membranes across three different length regimes: local−micrometer, micrometer−bulk, and local−bulk, which encompass all scales of the structural effects on the observed diffusion of water through the whole membrane. The local−micrometer tortuosity of the HEMA-*co*-MMA material is a factor of 3 larger than that for the HEA-*co*-EA material, indicating that the hydrophilic pathway network of HEA-*co*-EA exhibits a greater degree of connectivity. The uncertainty in the tortuosity values is ca. 6%.

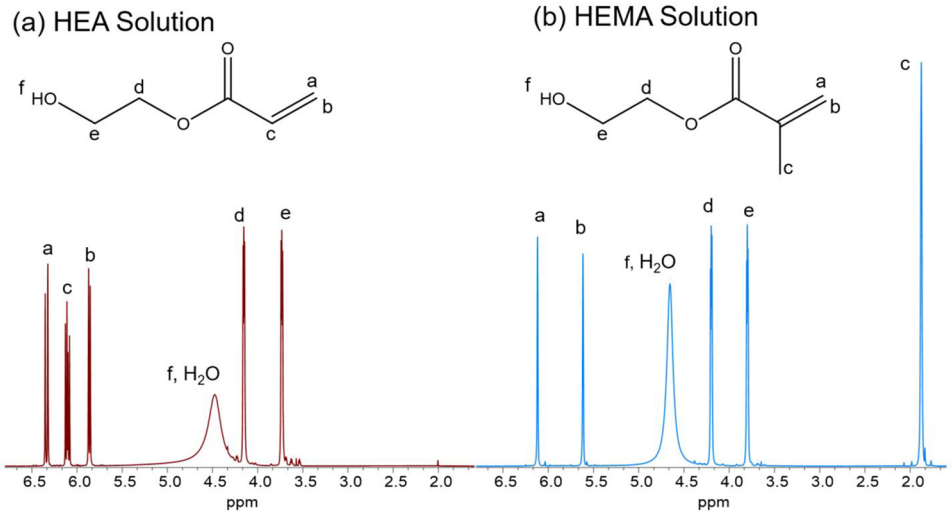

Figure 7. 1D spectra of the HEA (a, red) and HEMA solution (b, blue) analogues at 25 °C. We note the presence of an exchange-broadened peak in both spectra (peak f), with more pronounced broadening (≈ 100 Hz line width) and additional tailing of the signal downfield from the main peak in the HEA solution compared to the HEMA solution (≈ 45 Hz line width), indicating a faster exchange of proton magnetization between the monomer hydroxyl group and water in the HEMA solution at this temperature.

displacement of a water molecule during the prediffusion (inertial) time scale becomes small relative to spacing between polymer chains in the hydrated material, the local diffusion coefficient will approach that of pure water. Thus, our previous local−bulk tortuosity values also included the effects on diffusion from interactions between water and the hydrophilic groups along with the impacts of polymer morphology. In other words, our previous local−bulk tortuosity values therefore represented the total change to the diffusion coefficient of water as a result not only of polymer morphology and nanoconfinement but also of the interactions of water with the hydrophilic moieties of the membrane material. Here we revise this D_{loc} by using the D value measured using the analogue solutions (Figure 6) to more closely reflect the local molecular environment of the membrane materials in the absence of material structural/tortuosity effects. The tortuosity values reported here more accurately represent *only* the effects of the membrane water transport pathway structure on water transport across the different length-scale regimes. The relative factor difference in $\mathcal{T}_{L-B}$ between the two materials is similar to those previously reported, owing to the similar diffusivity of water in the two analogue solutions at 25 °C. In addition to local−bulk and micrometer−bulk tortuosity terms, we can define the local-to-micrometer tortuosity, $\mathcal{T}_{L-M}$ (eq 5).

$$\mathcal{T}_{L-M} = \frac{D_{loc}}{D_{\mu}} = \frac{\mathcal{T}_{L-B}}{\mathcal{T}_{M-B}} \tag{5}$$

$\mathcal{T}_{L-M}$ is simply the ratio of the other two tortuosity values and describes the relation of the local diffusion coefficient, D_{loc}, to the micrometer-scale diffusion coefficient, D_{μ}.The micrometer-scale diffusion coefficient, D_{μ} (represented as D_0 in our previous work),[7] is the diffusion coefficient of water measured at the shortest diffusion time (Δ) experimentally accessible by the NMR diffusometry instrumentation. As a result, the exact root-mean-squared diffusion length over which D_{μ} reports is somewhat variable with respect to the scale of the observed material heterogeneities. However, we feel it is useful here to delineate between the effects on water diffusion of the larger scale heterogeneities (that we believe originate from the

https://doi.org/10.1021/acs.macromol.1c01746
Macromolecules 2021, 54, 11187−11197

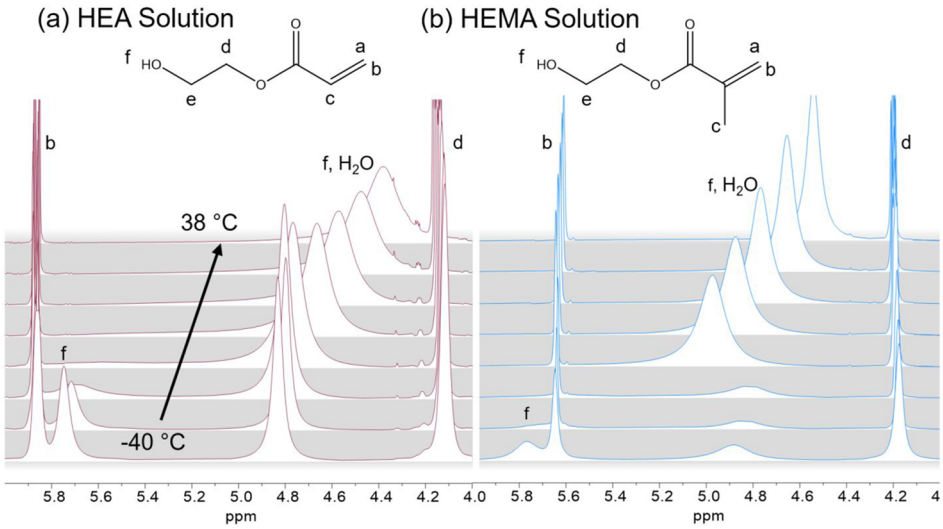

Figure 8. 1D spectra of the HEA−water (a, red) and HEMA−water (b, blue) analogue solutions; from −40 to 38 °C in 10 °C increments. The spectral intensities are normalized for peak d of each set of spectra individually and scaled to provide visibility of the exchange broadened peaks. In the HEA solution spectra we see at the lowest temperatures two relatively sharp peaks for the hydroxyl proton of the HEA molecule and water, whereas in the HEMA solution the corresponding peaks are more strongly broadened, indicating a faster rate of exchange between these two signals.

polymerization and membrane casting process) from the effects resulting from nanoconfinement. $\mathcal{T}_{L-M}$ encompasses both the effects of nanoconfinement and the material structure over the range 1−500 nm, whereas $\mathcal{T}_{M-B}$ reflects only larger scale structural heterogeneities. $\mathcal{T}_{L-B}$ now summarizes the entirety of the contributions to diffusion behavior that result from nanoconfinement and from all morphological impediments to water diffusion through the entire membrane material.

$\mathcal{T}_{L-M}$ measured for the HEMA-*co*-MMA material is a factor of 3 larger than that for the HEA-*co*-EA membrane (66.9 and 20, respectively), indicating a significantly less confined and more interconnected hydrophilic network in the HEA-*co*-EA material. Note that on length scales longer than E_a measurements can report (a few nanometers up to ∼0.5 μm), there is likely a significant difference in the polymer morphology heterogeneity, shown in the $\mathcal{T}_{L-M}$ values we have measured for these materials. While this difference in interconnectivity will affect the overall permeability of the materials, the water−salt selectivity should not be significantly affected by structures on length scales greater than the local (∼1 nm) scale. These analyses should serve to assist membrane synthesis experts in quantitatively informed design of next-generation molecular separation materials.

Chemical Exchange in Monomer−Water Solutions. In the membranes, water and polymer NMR signals are substantially broadened and overlapping due to the internal heterogeneities of the polymer structure.[7] This broadening obscures any useful molecular-level dynamics encoded into the NMR line shapes or positions. The initial goal in designing these two complementary membranes was that HEA and HEMA should interact with water similarly, based on the very similar chemical structures of both HEA and HEMA (Figure 1). However, in the room temperature 1D spectra of the HEMA and HEA analogue solutions (Figure 7), we observe the presence of heavily broadened (and in the case of the HEA−water solution, somewhat irregularly shaped) singlets at 4.66 and 4.48 ppm. These signals correspond to the protons of water combined (partially averaged) with the proton of the hydroxyl group of the two monomers. In particular, the markedly different appearance of the water/hydroxyl singlet between the two monomer−water solutions indicates a difference in the rate of water−monomer proton exchange between these solutions, and therefore a difference in the strength of the intermolecular interactions between water and the two monomers. The much broader singlet observed in the HEA−water solution spectra (Figure 7a; peak f,H_2O) along with the relatively large amount of signal intensity downfield of the peak in comparison to the HEMA−water spectra (Figure 7b) at the same temperature indicates that water and the hydroxyl group of the HEMA molecule are undergoing faster exchange than water and the HEA hydroxyl group. A key assumption is that the only two sites that protons are exchanging between are the water and the HEMA/HEA hydroxyl group. Aside from the carbonyl and ester oxygens, which could act as hydrogen bond acceptors and thereby exist as exchange sites, *J*-coupling and other nuclear spin interactions can additionally complicate the exchange from the assumed simple two-site model. As a confirmation of two-site exchange, we compare the spectra of the neat monomers, our analogue solutions, and dilute solutions of the monomers in DMSO-d_6 in Figure S4 and see that none of the other aliphatic protons appear to change significantly in their width, chemical shift, or multiplicity.

As we varied the temperature of the solutions through our diffusion studies, we noticed not only a change in the chemical shift of this signal (as is often seen with exchange-broadened singlets of hydroxyl groups) but additionally a change in peak shape. We obtained 1D spectra over a broader range for each of the analogue solutions, from −40 to 65 °C (Figure 8, with full temperature range presented in Figures S5 and S6), through which we see the progression of the hydroxyl and water signals from slow to fast exchange. These spectra follow the example shown in Figure S3b of an unequally populated exchange system.[29] From −40 to −10 °C, clearly defined peaks are observed for water and the hydroxyl groups in the spectra

https://doi.org/10.1021/acs.macromol.1c01746
Macromolecules 2021, 54, 11187−11197

of both analogue solutions, separated by 540 and 550 Hz in the HEMA and HEA−water solutions, respectively, with the hydroxyl peak in the HEMA−water solution heavily overlapping with peak b at −10 °C. In unequally populated exchange systems, an effect known as differential broadening is observed,[23,40,41] where the minor signal is more strongly broadened and shifted compared to the major peak, as the exchange rate increases up to the point of coalescence. This disparity in broadening and shift in peak positions increases with increasing difference in population between the signals as well as the separation of the two peaks in the absence of exchange. In our samples, we have a moderate difference in population (approximately 1:7 for both solutions) and a very large separation between the peaks (many observations of chemical exchange via NMR involve peak separations of ∼10 Hz). As a result, while a clearly defined peak might not be observed, there can be significant signal intensity in the region between the two peaks (Figure S7) or an irregular asymmetric shape of the observed peak. At coalescence, the two signals are indistinguishable, and only a single NMR peak is observed. The HEMA−water spectra transitions from having this significant intensity downfield of the single coalesced water/hydroxyl peak between −10 and −5 °C, whereas this change in the HEA−water spectra occurs between 40 and 45 °C. However, in the HEA solution the observed peak is significantly broader in the spectra below coalescence, and above coalescence the peak does not significantly narrow, resulting in greater uncertainty in the actual coalescence point of the exchanging peaks in this solution.

There are various methods for determining rate information from the exchange-broadened spectra. For simplicity, we employ a common approximation based on the relation between the difference in chemical shift frequency of the two signals in the absence of exchange, $\delta\nu$, to the overall exchange rate constant, k_{ex}, at the point of coalescence (the point at which the two signals become one indistinguishable peak) shown in eq 6.[23,32,42]

$$k_{ex} = \frac{\pi\delta\nu}{\sqrt{2}} \tag{6}$$

Using this relation and a measured peak separation of 550 Hz (HEA−water) and 540 Hz (HEMA−water) in the lowest temperature exchange spectra (Figure 8), we determine the exchange rate constant at the coalescence point for each solution to be ∼1100 s^{-1} for both solutions. Assuming that there are no fundamental changes in the exchange process over the observed temperature range, the exchange rates should increase with increasing temperature, and the observed exchange rate is faster in the HEMA−H_2O solution than the HEA−H_2O solution at all measured temperatures. A complete line shape analysis can be performed to determine more precise exchange rate constants for the entire temperature range and determine energetic parameters related to the exchange process,[23,41] but we will leave that to a future work focused on such details. While the chemical exchange and diffusive activation energies observed by NMR report on processes and interactions occurring on vastly different time scales (0.1−10 ms for the proton chemical exchange observed here versus the picoseconds to nanoseconds range for diffusive E_a), we note the relatively large differences in the interactions of water protons between these two apparently chemically similar hydrophilic monomers.

CONCLUSION

In summary, we have made detailed transport and dynamics measurements of two chemically similar acrylate-based and methacrylate-based separation membranes at similar hydration levels (≈10 wt %), in parallel with solutions mimicking each membrane's internal chemical environment. Through these investigations, we have shed light on the molecular-scale interactions and the various effects influencing water translational motion in these membranes. Measurements of the diffusive activation energy of water in aqueous solutions of the hydrophilic monomers HEMA and HEA model the local intermolecular environment of the membranes in the absence of any effects of polymer morphology or tortuosity. Comparison of the activation energy of water diffusion between membranes and their analogous solutions shows that there is a negligible difference in the effects of nanoconfinement on water transport between the HEA-*co*-EA and HEMA-*co*-MMA materials. We observe that water diffusion has a greater energetic cost (higher E_a) in the HEMA−water environment, but a greater number of configurations available for water diffusion to occur (through higher D_0) than in the HEA−water case. Additionally, with these solutions as a model of the local diffusion behavior in the membranes, we update our previous measurements of the local-to-bulk membrane tortuosity, which now represent more accurately the effects of the material transport pathway structure alone on water transport. Furthermore, through the observations of the exchange-broadened singlet corresponding to the protons chemically exchanging between water and monomer hydroxyl groups, we see that the HEMA−water interactions again differ from those between HEA and water. In terms of desalination performance, we believe that the increased local energetic cost to water diffusion in the HEMA−water environment is the dominant phenomenon by which the glassy HEMA-*co*-MMA material can more effectively separate salt from water. Finally, we believe that this approach to investigating the local transport environment of polymer separation materials, with and without the effects of geometric confinement, may be applicable to a wide range of complex or enigmatic polymer materials, including polyamide reverse osmosis materials.

ASSOCIATED CONTENT

Supporting Information

The Supporting Information is available free of charge at https://pubs.acs.org/doi/10.1021/acs.macromol.1c01746.

Additional diffusive Arrhenius plots, membrane permeability selectivity plot, and variable temperature ^{1}H NMR spectra demonstrating chemical exchange (PDF)

AUTHOR INFORMATION

Corresponding Author

Louis A. Madsen − *Department of Chemistry and Macromolecules Innovation Institute, Virginia Tech, Blacksburg, Virginia 24061, United States;* orcid.org/0000-0003-4588-5183; Email: lmadsen@vt.edu

Authors

Andrew G. Korovich − *Department of Chemistry and Macromolecules Innovation Institute, Virginia Tech, Blacksburg, Virginia 24061, United States;* orcid.org/0000-0003-3736-1523

https://doi.org/10.1021/acs.macromol.1c01746
Macromolecules 2021, 54, 11187−11197

Kevin Chang − *Department of Chemical Engineering, University of Virginia, Charlottesville, Virginia 22903, United States;* orcid.org/0000-0002-1320-9773

Geoffrey M. Geise − *Department of Chemical Engineering, University of Virginia, Charlottesville, Virginia 22903, United States;* orcid.org/0000-0002-5439-272X

Complete contact information is available at: https://pubs.acs.org/10.1021/acs.macromol.1c01746

Notes

The authors declare no competing financial interest.

■ ACKNOWLEDGMENTS

This research was supported by the National Science Foundation under Awards DMR 1810194 and CBET 1752048.

■ REFERENCES

(1) Park, H. B.; Kamcev, J.; Robeson, L. M.; Elimelech, M.; Freeman, B. D. Maximizing the right stuff: The trade-off between membrane permeability and selectivity. *Science* **2017**, *356* (6343), eaab0530.

(2) Cohen, Y.; Semiat, R.; Rahardianto, A. A perspective on reverse osmosis water desalination: Quest for sustainability. *AIChE J.* **2017**, *63* (6), 1771−1784.

(3) Fritzmann, C.; Löwenberg, J.; Wintgens, T.; Melin, T. State-of-the-art of reverse osmosis desalination. *Desalination* **2007**, *216* (1), 1−76.

(4) Geise, G. M.; Park, H. B.; Sagle, A. C.; Freeman, B. D.; McGrath, J. E. Water permeability and water/salt selectivity tradeoff in polymers for desalination. *J. Membr. Sci.* **2011**, *369* (1), 130−138.

(5) Hickner, M. A. Ion-containing polymers: new energy & clean water. *Mater. Today* **2010**, *13* (5), 34−41.

(6) Geise, G. M.; Lee, H.-S.; Miller, D. J.; Freeman, B. D.; McGrath, J. E.; Paul, D. R. Water purification by membranes: The role of polymer science. *J. Polym. Sci., Part B: Polym. Phys.* **2010**, *48* (15), 1685−1718.

(7) Chang, K.; Korovich, A.; Xue, T.; Morris, W. A.; Madsen, L. A.; Geise, G. M. Influence of Rubbery versus Glassy Backbone Dynamics on Multiscale Transport in Polymer Membranes. *Macromolecules* **2018**, *51* (22), 9222−9233.

(8) Allegrezza, A. E.; Parekh, B. S.; Parise, P. L.; Swiniarski, E. J.; White, J. L. Chlorine resistant polysulfone reverse osmosis modules. *Desalination* **1987**, *64*, 285−304.

(9) Park, H. B.; Freeman, B. D.; Zhang, Z.-B.; Sankir, M.; McGrath, J. E. Highly chlorine-tolerant polymers for desalination. *Angew. Chem., Int. Ed.* **2008**, *47* (32), 6019−6024.

(10) Glater, J.; Hong, S.-k.; Elimelech, M. The search for a chlorine-resistant reverse osmosis membrane. *Desalination* **1994**, *95* (3), 325−345.

(11) Zhang, H.; Geise, G. M. Modeling the water permeability and water/salt selectivity tradeoff in polymer membranes. *J. Membr. Sci.* **2016**, *520*, 790−800.

(12) Werber, J. R.; Deshmukh, A.; Elimelech, M. The critical need for increased selectivity, not increased water permeability, for desalination membranes. *Environ. Sci. Technol. Lett.* **2016**, *3* (4), 112−120.

(13) Geise, G. M.; Paul, D. R.; Freeman, B. D. Fundamental water and salt transport properties of polymeric materials. *Prog. Polym. Sci.* **2014**, *39* (1), 1−42.

(14) Lingwood, M. D.; Zhang, Z. Y.; Kidd, B. E.; McCreary, K. B.; Hou, J. B.; Madsen, L. A. Unraveling the local energetics of transport in a polymer ion conductor. *Chem. Commun.* **2013**, *49* (39), 4283−4285.

(15) Neves, L. A.; Sebastião, P. J.; Coelhoso, I. M.; Crespo, J. G. Proton NMR Relaxometry Study of Nafion Membranes Modified with Ionic Liquid Cations. *J. Phys. Chem. B* **2011**, *115* (27), 8713−8723.

(16) Chang, K.; Xue, T.; Geise, G. M. Increasing salt size selectivity in low water content polymers via polymer backbone dynamics. *J. Membr. Sci.* **2018**, *552*, 43−50.

(17) Thieu, L. M.; Zhu, L.; Korovich, A. G.; Hickner, M. A.; Madsen, L. A. Multiscale Tortuous Diffusion in Anion and Cation Exchange Membranes. *Macromolecules* **2019**, *52* (1), 24−35.

(18) Zhang, R.; Chen, Y.; Troya, D.; Madsen, L. A. Relating Geometric Nanoconfinement and Local Molecular Environment to Diffusion in Ionic Polymer Membranes. *Macromolecules* **2020**, *53* (9), 3296−3305.

(19) Kidd, B. E.; Forbey, S. J.; Steuber, F. W.; Moore, R. B.; Madsen, L. A. Multiscale Lithium and Counterion Transport in an Electrospun Polymer-Gel Electrolyte. *Macromolecules* **2015**, *48* (13), 4481−4490.

(20) Kreuer, K.-D.; Dippel, T.; Meyer, W.; Maier, J. Nafion® Membranes: Molecular Diffusion, Proton Conductivity and Proton Conduction Mechanism. *MRS Proceedings* **1992**, *293*, 273.

(21) Hammer, R.; Schönhoff, M.; Hansen, M. R. Comprehensive Picture of Water Dynamics in Nafion Membranes at Different Levels of Hydration. *J. Phys. Chem. B* **2019**, *123* (39), 8313−8324.

(22) Galitskaya, E.; Privalov, A. F.; Weigler, M.; Vogel, M.; Kashin, A.; Ryzhkin, M.; Sinitsyn, V. NMR diffusion studies of proton-exchange membranes in wide temperature range. *J. Membr. Sci.* **2020**, *596*, 117691.

(23) Sandström, J.; Sandström, J. S. *Dynamic NMR Spectroscopy*; Academic Press: 1982.

(24) Berg, U.; Sandström, J.; Jennings, W. B.; Randall, D. On the chirality of 2-hydroxy-NN-dialkythiobenzamides. Demonstration of three consecutive conformational processes. *J. Chem. Soc., Perkin Trans. 2* **1980**, No. 7, 949−956.

(25) Harvey, J. M.; Jackson, S. E.; Symons, M. C. R. Interactions in water-alcohol mixtures studied by NMR and infrared spectroscopy. *Chem. Phys. Lett.* **1977**, *47* (3), 440−441.

(26) Knispel, R. R.; Pintar, M. M. Temperature dependence of the proton exchange time in pure water by NMR. *Chem. Phys. Lett.* **1975**, *32* (2), 238−240.

(27) Luz, Z.; Meiboom, S. The Activation Energies of Proton Transfer Reactions in Water. *J. Am. Chem. Soc.* **1964**, *86* (22), 4768−4769.

(28) Luz, Z.; Meiboom, S. Nuclear Magnetic Resonance Study of the Protolysis of Trimethylammonium Ion in Aqueous Solution—Order of the Reaction with Respect to Solvent. *J. Chem. Phys.* **1963**, *39* (2), 366−370.

(29) Rogers, M. T.; Woodbrey, J. C. A PROTON MAGNETIC RESONANCE STUDY OF HINDERED INTERNAL ROTATION IN SOME SUBSTITUTED N,N-DIMETHYLAMIDES1. *J. Phys. Chem.* **1962**, *66* (3), 540−546.

(30) Luz, Z.; Gill, D.; Meiboom, S. NMR Study of the Protolysis Kinetics in Methanol and Ethanol. *J. Chem. Phys.* **1959**, *30* (6), 1540−1545.

(31) Graham, D. M.; Waugh, J. S. Nuclear Resonance Spectra of Rapidly Interconverting Rotational Isomers. *J. Chem. Phys.* **1957**, *27* (4), 968−969.

(32) Gutowsky, H. S.; Holm, C. H. Rate Processes and Nuclear Magnetic Resonance Spectra. II. Hindered Internal Rotation of Amides. *J. Chem. Phys.* **1956**, *25* (6), 1228−1234.

(33) Ammann, C.; Meier, P.; Merbach, A. A simple multinuclear NMR thermometer. *J. Magn. Reson. (1969-1992)* **1982**, *46* (2), 319−321.

(34) Hou, J. B.; Li, J.; Mountz, D.; Hull, M.; Madsen, L. A. Correlating morphology, proton conductivity, and water transport in polyelectrolyte-fluoropolymer blend membranes. *J. Membr. Sci.* **2013**, *448*, 292−299.

(35) Hou, J.; Li, J.; Madsen, L. A. Anisotropy and transport in poly(arylene ether sulfone) hydrophilic−hydrophobic block copolymers. *Macromolecules* **2010**, *43* (1), 347−353.

(36) Jerschow, A.; Müller, N. Suppression of Convection Artifacts in Stimulated-Echo Diffusion Experiments. Double-Stimulated-Echo Experiments. *J. Magn. Reson.* **1997**, *125* (2), 372−375.
(37) Hoffman, R. E.; Becker, E. D. Temperature dependence of the 1H chemical shift of tetramethylsilane in chloroform, methanol, and dimethylsulfoxide. *J. Magn. Reson.* **2005**, *176* (1), 87−98.
(38) Van Geet, A. L. Calibration of methanol nuclear magnetic resonance thermometer at low temperature. *Anal. Chem.* **1970**, *42* (6), 679−680.
(39) Chan, E. P.; Frieberg, B. R.; Ito, K.; Tarver, J.; Tyagi, M.; Zhang, W.; Coughlin, E. B.; Stafford, C. M.; Roy, A.; Rosenberg, S.; Soles, C. L. Insights into the Water Transport Mechanism in Polymeric Membranes from Neutron Scattering. *Macromolecules* **2020**, *53* (4), 1443−1450.
(40) Höfner, D.; Lesko, S. A.; Binsch, G. Dynamic proton magnetic resonance studies on complex spin systems. Non-mutual three-spin exchange in four 1-substituted cyclohexanes-2,2,3,3,4,4,5,5-d8 and mutual four-spin exchange in cyclohexane-1,1,2,2,3,3,4,4-d8. *Org. Magn. Reson.* **1978**, *11* (4), 179−196.
(41) Okazawa, N.; Sorensen, T. S. The line-shape analysis of nuclear magnetic resonance peaks broadened by the presence of a 'hidden' exchange partner. *Can. J. Chem.* **1978**, *56* (21), 2737−2742.
(42) Kost, D.; Carlson, E. H.; Raban, M. The validity of approximate equations for kc in dynamic nuclear magnetic resonance. *J. Chem. Soc. D* **1971**, No. 13, 656−657.

https://doi.org/10.1021/acs.macromol.1c01746
Macromolecules 2021, 54, 11187−11197